Materials and Manufacturing Processes, 27: 1457–1461, 2012
Copyright © Taylor & Francis Group, LLC
ISSN: 1042-6914 print/1532-2475 online
DOI: 10.1080/10426914.2012.677914

Taylor & Francis
Taylor & Francis Group

Effects of Activating Flux on Weld Bead Geometry of Inconel 718 Alloy TIG Welds

Hsuan-Liang Lin[1] and Tong-Min Wu[2]

[1]*Army Academy R.O.C., Vehicle Engineering, Jungli, Taoyuan, Taiwan*
[2]*National Chiao Tung University, Mechanical Engineering, Hsinchu, Taiwan*

The purpose of this work is to investigate the effects of activating fluxes and welding parameter to the penetration and depth-to-width ratio (DWR) of weld bead of Inconel 718 alloy welds in the tungsten inert gas (TIG) welding process. In the activating flux with TIG (A-TIG) welding process, the single-component fluxes used in the initial experiment were SiO_2, NiO, MoO_3, Cr_2O_3, TiO_2, MnO_2, ZnO, and MoS_2. Based on the higher DWR of weld bead, four fluxes were selected to create six new mixtures using 50% of each original flux. The A-TIG weldment coated 50% SiO_2 + 50% MoO_3 flux and 75° of electrode tip angle were provided with better welding performance. In addition, the experimental procedure of flux-bounded TIG (FB-TIG) welding with the same welding conditions and flux produced full penetration of weld bead on a 6.35 mm thickness of Inconel 718 alloy plate with single pass weld.

Keywords Coatings; Flux; Geometry; High-temperature; Nonferrous; Optimization; Weldability; Welding.

Introduction

Inconel 718 alloy is one of the most widely used nickel-based alloys due to its superior mechanical property and oxidation resistance at high temperature in aerospace, power, and nuclear industries. Electron beam (EB), laser beam (LB), and tungsten inert gas (TIG) welding were known to play important roles in aerospace, military, power plants, and automotive industries. A lot of researches about EB and LB welding on Inconel 718 alloy have been performed because that energy density in these welding is extremely high. A higher depth-to-width ratio (DWR) of weld bead geometry can be easily obtained with small heat input in EB and LB welding process [1–3]. A few published reports are available on TIG welding of Inconel 718 alloy focus on selection of welding parameters for obtaining optimal weld bead geometry. The TIG welding is one of the mainly applied welding processes in industry to nonferrous and stainless steels for high quality weld and low investment. The welding quality is strongly characterized by the weld bead geometry. The weld bead geometry plays an important role in determining the mechanical properties of the weld [4]. However, the relatively shallow penetration capability and low productivity are the main disadvantage in the TIG welding process. Achieving full penetration of welds and increasing productivity are the main objectives in the welding industry. In order to achieve single pass welds with no edge preparation, instead of multipass procedures, one of the most notable techniques is to use activating flux with TIG (A-TIG) welding process [5], as shown in Fig. 1a. Chandrasekhar et al. [6] proved that an intelligent methodology based on genetic algorithm has been developed to optimize the A-TIG process parameters to achieve the target weld bead geometry for welding of type 304LN and 316LN stainless steels. Vasudevan [7] used soft computing techniques for modeling and prediction of microstructures of stainless steel welds, modeling weld bead geometry, optimization of A-TIG, and TIG welding process parameters to tailor the weld bead geometry in stainless steel welds. Lin et al. [8] demonstrated that the highest DWR of low carbon steel and stainless steel butt-joint weld bead can be obtained in A-TIG process using 18% TiO_2 and 82% SiO_2 mixed flux. In addition, activating flux is also employed in a new technique called flux bounded-TIG (FB-TIG) to weld aluminum alloy and 304 L stainless steel. In FB-TIG configuration, two separated coatings are applied and the gap between coatings with different size, as shown in Fig. 1b. Sire et al. [9] demonstrated that 6 mm thickness penetration in FB-TIG welding process was obtained at the same welding conditions compared to about 3 mm in conventional TIG welding. Both weld penetrations and DWR are higher (about twice) with FB-TIG welding. Rückert et al. [10] showed that the silica coating thickness window is very narrow in A-TIG of 304 L stainless steel welds. The FB-TIG configuration allows of obtaining comparable results for thicker deposits with enlarging of coating thickness. The sensitivity of weld penetration with coating thickness is thus reduced in FB-TIG process.

The purpose of this work is to investigate the effect of both the activating flux and the major welding parameters on the weld bead geometry of the Inconel 718 alloy welds. First, the single-component flux was used to evaluate the effects of weld bead geometry. Then,

Received January 2, 2012; Accepted March 12, 2012

Address correspondence to Hsuan-Liang Lin, Army Academy R.O.C., Vehicle Engineering, No. 750, Long-dong Rd., Jungli, Taoyuan, Taiwan; E-mail: alaniin@ms47.hinet.net

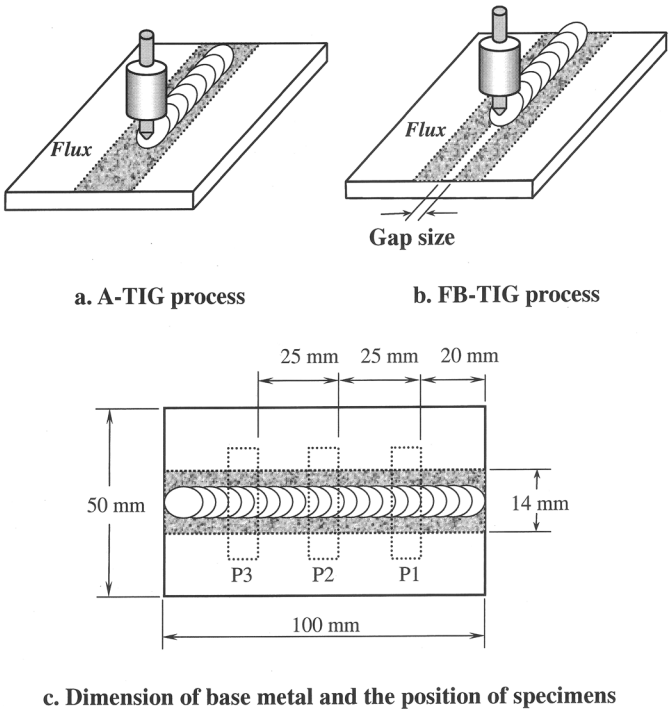

FIGURE 1.—The A-TIG and FB-TIG welding process and its base metal.

mixed-component flux was used to improve the weld bead geometry of Inconel 718 welds and analyze the effect of parameters such as welding current and electrode tip angle in the A-TIG process. The objective of this work is also to compare the penetration and DWR of Inconel 718 alloy welds obtained in A-TIG and FB-TIG welding process.

EXPERIMENTAL PROCEDURE

Inconel 718 alloy sheets with dimensions 50 (100 (6.35 mm were prepared for this study; its chemical composition is listed in Table 1. A EWTh-2 electrode was used to produce a bead-on-plate weld, as shown in Fig. 1. Before TIG welding, the activating flux was mixed with methanol to produce a paint-like consistency, a layer thickness of approximately 0.2 mm, is applied to the surface of base metal to be welded by means of a brush. The single-component fluxes used in the initial experiment were SiO_2, NiO, MoO_3, Cr_2O_3, TiO_2, MnO_2, ZnO, and MoS_2. In this work, measurements of the weld bead geometry were performed for evaluation of the quality of activating flux TIG welds of Inconel 718 alloy. It took the width of weld bead and the depth of penetration to describe the weld bead geometry. The DWR of the weld bead geometry of each specimen was selected as the quality characteristic of TIG welding process. An optical microscope was used to measure the depth and width of weld bead geometry of each specimen. All metallographic specimens as shown in Fig. 1c were prepared by mechanical lapping, grinding and polishing to a 0.3 μm finish, followed by etching in a solution containing 2 g of $CuCl_2$, 40 ml of CH_3OH, and 35 ml of HCl.

TABLE 1.—Chemical concentration of each element in Inconel 718 alloy.

Element	Ni	Cr	Nb + Ta	Mo	Ti	Al	Co	C	Mn	Si	Fe
Wt%	55.0	21.0	5.5	3.3	1.15	0.8	1.0	0.05	0.35	0.35	Balance

RESULTS AND DISCUSSION

Effect of Single-Component Flux

The previous studies [11–14] have revealed that the activating fluxes lead to an increased penetration of weld bead may have two types of action: namely, the Marangoni convection and the electric arc behavior. Some researchers [13, 14] believe that the main mechanism in the weld pool is the Marangoni convection. In traditional TIG welding without activating flux, the temperature coefficient of surface tension on the molten pool generally exhibited a negative value. If the surface tension (σ) in the pool center is lower than the temperature at the pool edge, then the surface tension gradient ($\partial\sigma/\partial T$) generates Marangoni convection with the fluid flows from the pool center to the edge in the molten pool, yielding a wide and shallow TIG welds as shown in Fig. 2a. In A-TIG welding with activating fluxes,

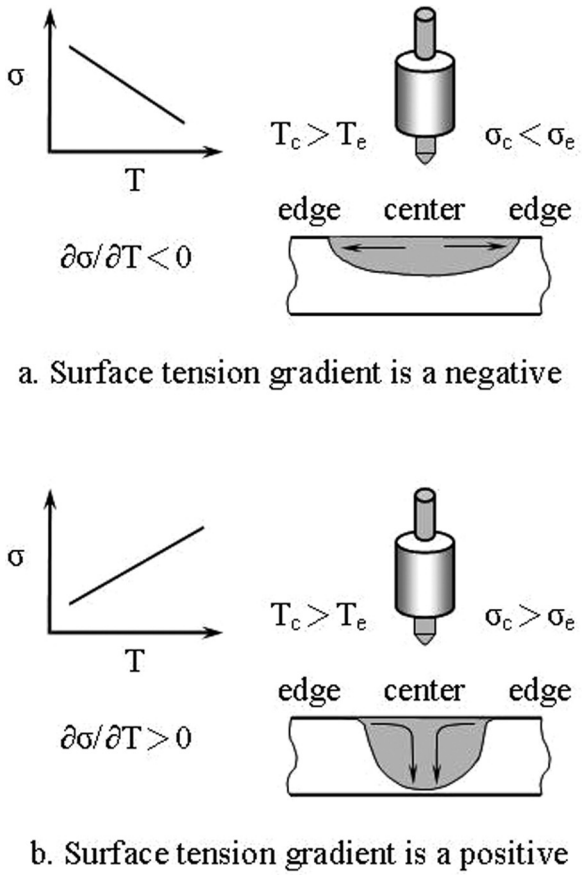

FIGURE 2.—Marangoni convection mode by surface tension gradient.

TABLE 2.—Welding parameters for initial experiments.

Welding current	170 A
Travel speed	150 mm/min
Arc length	2.0 mm
Diameter of electrode	3.2 mm
Angle of electrode tip	60°
Flow rate of shield gas	14 L/min

the temperature coefficient of surface tension on the molten pool changed from a negative to a positive value. Therefore, the surface tension at the pool center is higher than at the pool edge. This indicated that the surface tension gradient change the direction of the fluid flow in the molten pool, a relatively deeper and narrower weld is produced as shown in Fig. 2b.

In this work, the welding parameters used in the initial experiment are given in Table 2. Figure 3a shows the DWR of weld bead geometry of Inconel 718 alloy made by the TIG welding process without activating flux and with different single-component fluxes. The penetration capability of A-TIG welds was obviously higher than that of the traditional TIG welds without activating flux. A-TIG welding with single-component fluxes such as SiO_2, NiO, MoS_2, and MoO_3 fluxes produced a significant Marangoni convection and increase the penetration and DWR of Inconel 718 alloy welds. It was found that undercut was observed on the weld bead surface of Inconel 718 alloy welds using MoS_2 flux as shown in Fig. 3b.

Effect of Mixed-Component Flux

Based on the higher DWR of specimens, four single component fluxes were selected to mix with each other using 50% weight percent each. The mixed component fluxes were SiO_2-MoO_3, SiO_2-NiO, MoO_3-NiO, SiO_2-MoS_2, MoS_2-NiO, and MoS_2-MoO_3, and the mixed component fluxes were used for investigating the effect to the DWR of specimens. Figure 4a shows the penetration and DWR of weld bead geometry using the mixed-component fluxes. Comparison of Fig. 3a with Fig. 4a, the DWR of specimens of mixed activating flux TIG welds were higher than that of the welds using

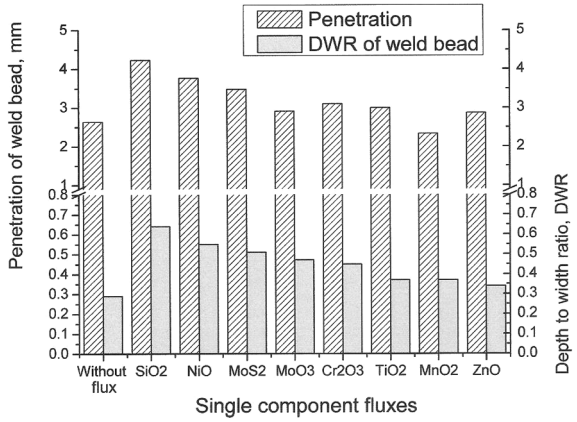

a. Weld bead geometry of welds in A-TIG process

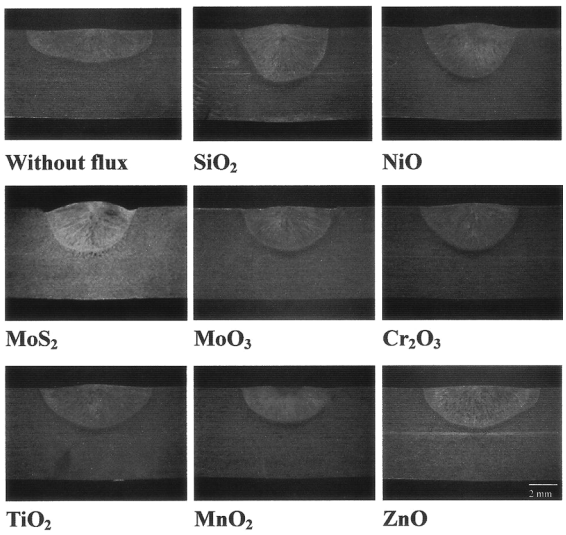

b. Cross-section of welds in A-TIG process

FIGURE 3.—Effect of single component flux on TIG welds.

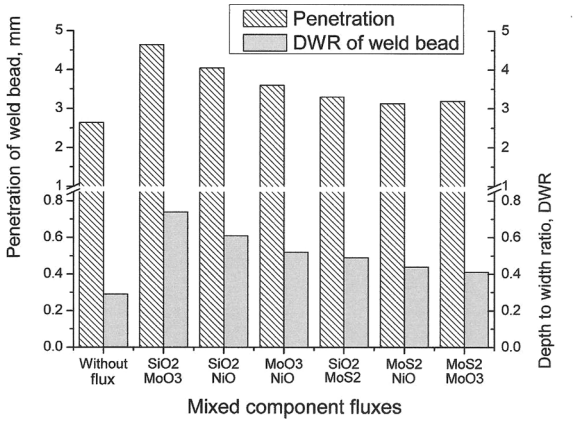

a. Weld bead geometry of welds in A-TIG process

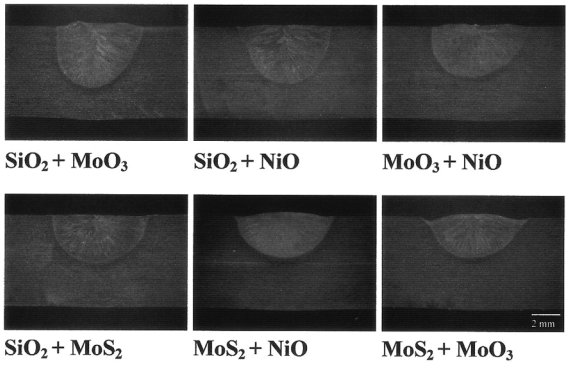

b. Cross-section of welds in A-TIG process

FIGURE 4.—Effect of mixed component flux on TIG welds.

single-component fluxes, with the oxide 50% SiO_2 + 50% MoO_3 mixed flux being the most significant. It was also found that undercut was observed on the weld bead surface of Inconel 718 alloy welds using 50% MoS_2 + 50% MoO_3 mixed flux as shown in Fig. 4b. However, MoS_2 flux mixed with the other activating flux that produced a significant Marangoni convection such as SiO_2 flux, the undercut not occur in the cross-section of Inconel 718 alloy weld bead, as shown in Fig. 4b.

Effect of Welding Parameters

Huang [15] proved that a mixed component flux, including 30% TiO_2, 25% SiO_2, 25% Cr_2O_3, and 20% MoO_3, has the most effect on the penetration and DWR of weld bead increased with higher welding current in the A-TIG welds of JIS 304 stainless steel. Therefore, the 50% SiO_2 + 50% MoO_3 mixed flux was used to improve the weld bead geometry of Inconel 718 welds and analyze the effect of welding current in the A-TIG welding process. Figure 5a shows that the relationship between weld bead geometry and welding current. It indicated that the penetration and DWR of Inconel 718 alloy welds are best when the welding current is adjusted from 170 to 180 A in this A-TIG welding process. The previous experiment [16] showed that the most significant parameters for DWR of weld bead geometry are welding current and electrode tip angle in TIG welding process. The angle of electrode tip is a major parameter that affects the penetration and DWR of weld bead geometry in the TIG welding process. Goodarzi et al. [17] developed a mathematical model to study the effect of the electrode tip angle on the weld pool properties. The information required to simulate the flow including the heat flux to the workpiece, the input current density, and the gas shear stress, was derived from the arc model. It is found that the buoyancy and electromagnetic forces do not play major roles in determining the flow pattern. Instead, the relative magnitude of the gas shear stress and the surface tension and also the sign of the surface tension determine the flow pattern in the weld pool. The electrode tip angle which alters the gas shear stress and especially the heat flux to the workpiece can produce a significant change in the overall shape and size of the weld pool. In this work, the 50% SiO_2 + 50% MoO_3 mixed flux and welding current at 180 A were used to analyze the effect of electrode tip angle. Figure 5b shows that the relationship between weld bead geometry and electrode tip angle. It indicated that the penetration and DWR of Inconel 718 alloy welds are best when the electrode tip

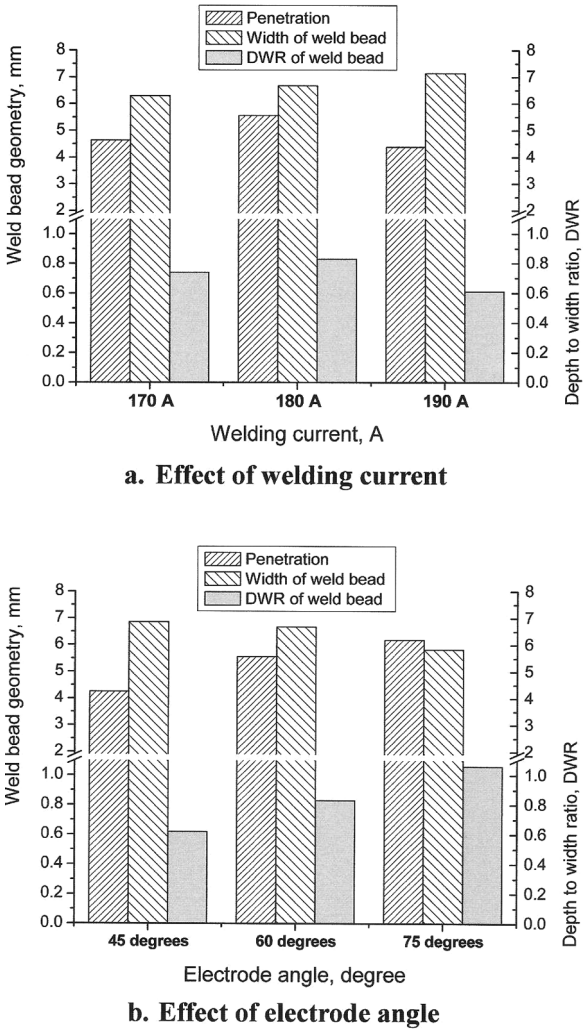

FIGURE 5.—Effect of major welding parameters on A-TIG welds.

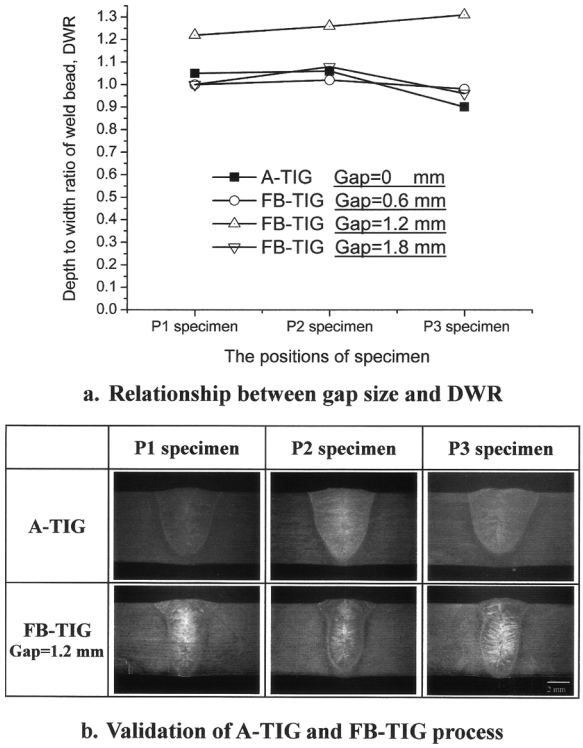

FIGURE 6.—Effect of gap size on FB-TIG welds.

angle is adjusted from 60 to 75 degrees in A-TIG process.

Effect of Gap Size in FB-TIG

The flux in FB-TIG is applied not as a single cover, but as a set of two parallel coatings, as shown in Fig. 1b. Electrical resistivity of the flux is supposed to channel the incoming electrons onto the central metallic zone exempt from the flux coating. The concept of two separate coatings is also attractive from perspectives of flux consumption if weld penetrations comparable to A-TIG can be obtained over a broad range of coating thickness. Rückert et al. [10] demonstrated that the penetration of 304 L stainless steel welds via FB-TIG process higher than that of the welds via A-TIG process using the same silica coating thickness and welding current. Figure 6a shows the effect of gap size on the DWR of Inconel 718 alloy welds. It indicates that the DWR of specimens is best when the gap size was set to 1.2 mm in the FB-TIG process. Comparison of A-TIG with FB-TIG as shown in Fig. 6b demonstrates that the weld bead geometry of Inconel 718 welds via the FB-TIG are slender than that applying A-TIG process.

Conclusions

TIG welding with single component fluxes such as SiO_2, NiO, MoS_2, and MoO_3 fluxes, and mixed component fluxes such as 50% $SiO_2 + 50\%MoO_3$ and 50% $SiO_2 + 50\%$ NiO produced a significant increase the penetration and DWR of Inconel 718 alloy welds. However, the undercut of specimen was observed on the weld bead surface of Inconel 718 alloy welds using MoS_2 flux. The improvement of the DWR of Inconel 718 alloy welds from 60 to 75 degrees of electrode angle is 28%. This work demonstrates that the weld bead geometry of Inconel 718 welds via the FB-TIG with 1.2 mm gap are slender than that applying A-TIG process. The FB-TIG process produced full penetration in 6.35 mm-thickness of Inconel 718 alloy plate with single pass weld.

Acknowledgment

The authors gratefully acknowledge the financial support for this research provided by the National Science Council, Taiwan, Republic of China, under the Grant No. NSC 98-2221-E-539-001.

Reference

1. Huang, C.A.; Wang, T.H.; Lee, C.H.; Han, W.C. A study of the heat-affected zone (HAZ) of an Inconel 718 sheet welded with electron-beam welding (EBW). *Materials Science and Engineering A* **2005**, *398*, 275–281.
2. Madhusudhana Reddy, G.; Srinivasa Murthy, C.V.; Srinivasa Rao, K.; Prasad Rao, K. Improvement of mechanical properties of Inconel 718 electron beam welds- influence of welding techniques and postweld heat treatment. *International Journal of Advanced Manufacturing Technology* **2009**, *43*, 671–680.
3. Janaki Ram, G.D.; Vanugopal Reddy, A.; Prasad Rao, K.; Reddy, G.M.; Sarin Sundar, J.K. Microstructure and tensile properties of Inconel 718 pulsed Nd-YAG laser welds. *Journal of Materials Processing Technology* **2005**, *167*, 73–82.
4. Pal, S.; Pal, S.K.; Samantaray, A.K. Determination of optimal pulse metal inert gas welding parameters with a Neuro-GA technique. *Materials and Manufacturing Processes* **2010**, *25*, 606–615.
5. Tseng, K.H.; Hsu, C.Y. Performance of activated TIG process in austenitic stainless steel welds. *Journal of Materials Processing Technology* **2011**, *211*, 503–512.
6. Chandrasekhar, N.; Vasudevan, M. Intelligent modeling for optimization of A-TIG welding process. *Materials and Manufacturing Processes* **2010**, *25*, 1341–1350.
7. Vasudevan, M. Soft computing techniques in stainless steel welding. *Materials and Manufacturing Processes* **2009**, *24*, 209–218.
8. Lin, H.L.; Chou, C.P. Optimization of the GTA welding process using combination of the Taguchi method and a neural-genetic approach. *Materials and Manufacturing Processes* **2010**, *25*, 631–636.
9. Sire, S.; Marya, S. On the selective silica application to improve welding performance of the tungsten arc process for a plain carbon steel and for aluminum. *Comptes Rendus Mecanique* **2002**, *330*, 83–89.
10. Rückert, G.; Huneau, B.; Marya, S. Optimizing the design of silica coating for productivity gains during the TIG Welding of 304 L stainless steel. *Materials and Design* **2007**, *28* (9), 2387–2393.
11. Leconte, S.; Paillard, P.; Chapelle, P.; Henrion, G.; Saindrenan, J. Effect of oxide fluxes on activation mechanisms of tungsten inert gas process. *Science and Technology of Welding and Joining* **2006**, *11* (4), 389–397.
12. Leconte, S.; Paillard, P.; Saindrenan, J. Effect of fluxes containing oxides on tungsten inert gas welding process. *Science and Technology of Welding and Joining* **2006**, *11* (1), 43–47.
13. Xu, Y.L.; Dong, Z.B.; Wei, Y.H.; Yang, C.L. Marangoni convection and weld shape variation in A-TIG welding process. *Theoretical and Applied Fracture Mechanics* **2007**, *48*, 178–186.
14. Lu, S.; Fujii, H.; Sugiyama, H.; Nogi, K. Mechanism and optimization of oxide fluxes for deep penetration in gas tungsten arc welding. *Metallurgical and Materials Transations A* **2003**, *34A*, 1901–1907.
15. Huang, H.Y. Research on the activating flux gas tungsten arc welding and plasma arc welding for stainless steel. *Metals and Materials International* **2010**, *16* (5), 819–825.
16. Lin, H.L.; Chou, C.P. Optimisation of the GTA welding process using the Taguchi method and a neural network. *Science and Technology of Welding and Joining* **2006**, *11* (1), 120–126.
17. Goodarzi, M.; Choo, R.; Takasu, T.; Toguri, J.M. The effect of the cathode tip angle on the gas tungsten arc welding arc and weld pool: II. The mathematical model for the weld pool. *Journal of Physics D: Applied Physics* **1998**, *31*, 569–583.